

Research Article

Microdrilling Studies PLA/Bronze Composite Samples Printed Using Fused Deposition Model

P. Sneha ¹, K. Balamurugan ^{1,2}, Y. Jyothi ¹ and Santhosh Krishnan ³

¹Department of Mechanical Engineering, VFSTR (Deemed to be University), Guntur 522213, Andhra Pradesh, India

²Department of Mechanical Engineering, SRM Madurai College for Engineering and Technology, Pottapalayam 630612, Tamil Nadu, India

³Department of Mechatronics Engineering, Wollo University, Kombolcha Institute of Technology, Post Box No: 208, Kombolcha, Ethiopia

Correspondence should be addressed to K. Balamurugan; kbalan2000@gmail.com and Santhosh Krishnan; santhosh@kiot.edu.et

Received 5 August 2022; Revised 10 December 2022; Accepted 6 April 2023; Published 20 June 2023

Academic Editor: Khan M. Adam

Copyright © 2023 P. Sneha et al. This is an open access article distributed under the Creative Commons Attribution License, which permits unrestricted use, distribution, and reproduction in any medium, provided the original work is properly cited.

Fused deposition models (FDMs) are the latest trends for constructing complicated and instinctive 3D printing. Polylactic acid (PLA) is the most widely used raw material in extrusion-based three-dimensional (3D) printing in many areas since it is biodegradable and environmentally friendly; however, its utilization is limited due to some of its disadvantages such as mechanical weakness and water solubility rate. To increase the mechanical properties of the FDM, nano bronze particles have been added as advanced research. Printing the hole less than a millimetre is complicated, and there is a limited report available in FDM. In this paper, polylactic acid (PLA) with a 14% bronze composite filament is made by hot extruding under the desired FDM conditions. The samples are built with 100% infilled density with 45° orientation to a sample size of 50 × 50 × 10 mm. To examine the printing state and the effect of microdrilling on the printed specimen, two different specimens are printed with and without holes. An industrial drill with specified feed, speed, and cutting width is used to perform the test. The size of the drilled hole is checked by scanning electron microscopy. The quality of the drilled hole and the wear of the tool is investigated and reported. According to the observation, it is noted that the secondary machining operation becomes unavoidable to have a hole of less than a millimetre. Machining, cutting speed, and feed speed influence the delamination zone and the circumference of the hole.

1. Introduction

For any component, the drilling operation is essential for connecting two components. In general, the measurement of machining is based on the conditions and characteristics of the sample. The delamination size and surface roughness of the sample are checked by analysing the different tool wear observed under drilling conditions. Defects which occur during the drilling operation on polymer matrix materials depend on the machining conditions due to the condition of the test specimen [1]. Now, one-day drilling operations are performed on polymer materials such as carbon fibre-reinforced matrix, glass fibre-reinforced matrix, and ceramic nanoparticle-reinforced matrix. Printing holes smaller than 1 mm in diameter is the most challenging task in the FDM [2].

The study explains that the characteristics of polymer matrix composites in the drilling process depend largely on the machining parameters and the tool used [3]. To improve the delamination effect, the spindle speed shows the significant effect on (polymer matrix composite) PMC-strengthened carbon nanotubes [4]. However, a greater effect is observed with the chopped fibre and the PMC nanoreinforced material. The circumference of the hole with surface defects is recorded during microdrilling [5]. Sudden tool breakage and excess tool wear are observed on nanoparticle-reinforced PMC; owing to the presence of hard elements, the tool witnesses the sudden work load that drastically determines the tool life [6].

The geometry of the cutting tool and the pushing force has a significant effect on the delamination of fibre glass-

reinforced composite (GFRC) [7]. The analysis of the damage sustained during the drilling of biocomposite with various machining parameters leads to better fraying and better interface cohesion [8]. The study on microdrilling of oil hardening and nonshrinking (OHN) steel using an HSS drill shows that the reduction of errors during drilling can provide better performance [9]. The input and output pressure of the drill bit will have an effect on the circularity of carbon fibre-reinforced PMCs in drilling operations [10].

The state of processing of composites is determined by chip formation and drill cutting parameters for thermoplastics and thermosets [11]. The delamination effect and surface roughness depend on the formation of the microchip and its form [12]. PMC faces the kerf angle by increasing the thickness of the specimens. The formation of burrs in the surface of the composite material will significantly reduce the output performance of the machining condition and is characterized and reported [13]. Due to the low thermal conductivity, PMC faces a hole shrinkage during the machining operation that greatly determines the quality of drill holes [14]. To enhance drilling operation on carbon fibre-reinforced PMCs, thrust force can be considerably reduced with varied machining angles, thereby reducing the effect of the tool wear [15].

Additive manufacturing has enormous advantages which contribute significantly to the thickness performance of the inner layer as part of the FDM process which shows the performance of 3D printed samples [16]. Clustering of the reinforcement of the matrix provides additional work load to the tool and causes excessive wear that determines the surface irregularity of the sample [17]. For example, when carbon nanotube-PLA composite samples undergo microdrilling, the tool faces excessive wear and even breaks owing to the application of the load [18]. The effect of the drilling machining parameters in epoxy composite materials deals with the behaviour of the delamination, surface roughness of the matrix at extreme speed, and feed conditions [19]. The microlevel holes are essential for several engineering applications but the hole built at microlevel using 3D fused filament fabrication (FFF) process is a challenging task [20]. The machining characteristics of the reinforced jute fibre PMC show that the drilling force and the pushing force on the delaminating area are examined by SEM. The analysis confirms that the bonding between the reinforcement and the matrix significantly affects the machining conditions [21].

The inherent characteristics of fiberglass-reinforced plastic composites perform the drilling operation in accordance with various parameters. The effects of drilled geometry and driving forces are studied [22]. Using unconventional methods in tool design, the behaviour of fibre-reinforced plastics is used in enormous applications. By comparing numerical values, the geometry of the drill explains that the characteristics of a fibre-reinforced polymer (FRP) laminate play an important role in the results of a qualitative method [23]. The study of carbon fibre-reinforced composite (CFRP) material on thermal behaviour and the mechanism of fatigue by optical morphology leads to fatigue performance determining the properties of

materials [24]. It investigates the wear mechanism of the tungsten carbide drill and evaluates the speeds; the behaviour of the mechanism can be shown by delaminating a drilled hole. The effects are demonstrated through the cutting forces [25].

In this work, the PLA-14% of the bronze composite filament is successfully extruded and used as a printing filament to identify printing conditions in the FDM at the standard size. For benchmarking, samples are printed with or without holes. Standard operating procedure for drilling the test sample is performed. The importance of the processing condition based on the hole's geometry is studied by scanning electron microscopy (SEM) and is reported. The tool wear characterisation study is also completed and reported.

2. Materials and Methods

2.1. PLA-14% Bz Composite Filament Preparation. The primary investigation is conducted with varied bronze particles of size 80 to 90 nm in the PLA matrix. The report suggests that adding 14% Bz as reinforcement in PLA matrix will yield a proper dispersion composite filament for the 3D printed application. Here, the agglomeration is a difficult task with increased reinforcement [26]. Bz with less than 18% will reduce the mechanical property of the samples, and it was reported from the earlier study, with the varied weight percentage of Bz of 6, 10, 14, and 18 [27]. Bronze having various weight percentages of 0, 6, 10, 14, and 18 is added to the matrix as shown in Figure 1. PLA billets are powdered by means of commercially available ball milling process. Coimbatore Metal Market in Coimbatore, India, has supplied bronze with a particle diameter of 80–90 nm. The combination is softened by an increase in temperature to about 190°C while maintaining a constant thread velocity of 300 RPM. The solution is transferred into a hopper and extruded to create a 1.25 mm diameter 3D filament mix. To ensure a steady flow of PLA material with bronze particles, the extruder is kept at a temperature of 60°C.

To confirm filament use, it must be manufactured using the same FDM-machined settings as shown in Table 1. To determine the appropriate bronze weight% in the matrix material, densities, modulus of rupture, strength properties, tensile strength, and flexural modulus are determined. Figure 2 depicts a typical optical image of a cross-section of 3D composite filaments that were measured at 50x. As the fraction of metallic particles in the contents increases, the particles become more agglomerating and clustered. Obtaining a continuous 3D composite filament when more than 20% reinforcements are added becomes a difficult task. As a result, the greatest amount of reinforcements in the matrix material is set at 18%.

Tensile and flexural strength decreased along with the reduction of elongation because of the addition of bronze reinforcement. However, the hard Bz elements withstand extra load bearing capacity in compression test, and it can be verified from Table 1. The printed samples are subjected to basic mechanical tests such as deformation, compression, and flexural tests. Increased reinforcement leads to metal

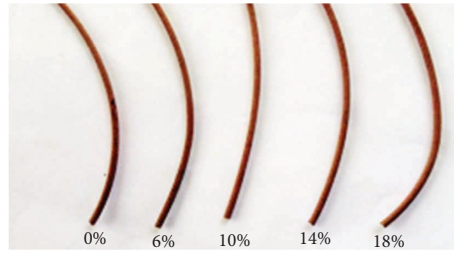


FIGURE 1: Bronze filament with varied composition in the PLA matrix.

TABLE 1: Properties of PLA/x% of Bz.

Measurement components	Percentage of bronze				
	0	6	10	14	18
Softening temperature T_m (°C)	160	160	160	160	160
Bed temperature (°C)	40	40	40	40	40
Filling velocity (mm/min)	20	20	20	20	20
Airgap (mm)	0	0	0	0	0
Infill (%)	100	100	100	100	100
Raster angle (deg)	45	45	45	45	45
Density ρ (g/cm ³)	1.25	1.65	1.84	2.11	2.64
Elongation at break (%)	6	5.4 ± 1.6	5.1 ± 1.6	4.3 ± 1.2	3.9 ± 1.8
Compressive strength (peak) (MPa)	17.9	18.9	19.4	20.6	21.4
Tensile strength (peak) (MPa)	46.8	41.8 ± 2.5	39.4 ± 1.5	34.9 ± 2	31.4 ± 2
Flexural strength (peak) (MPa)	61.8	60.4 ± 2	58 ± 1	56 ± 2	53 ± 2

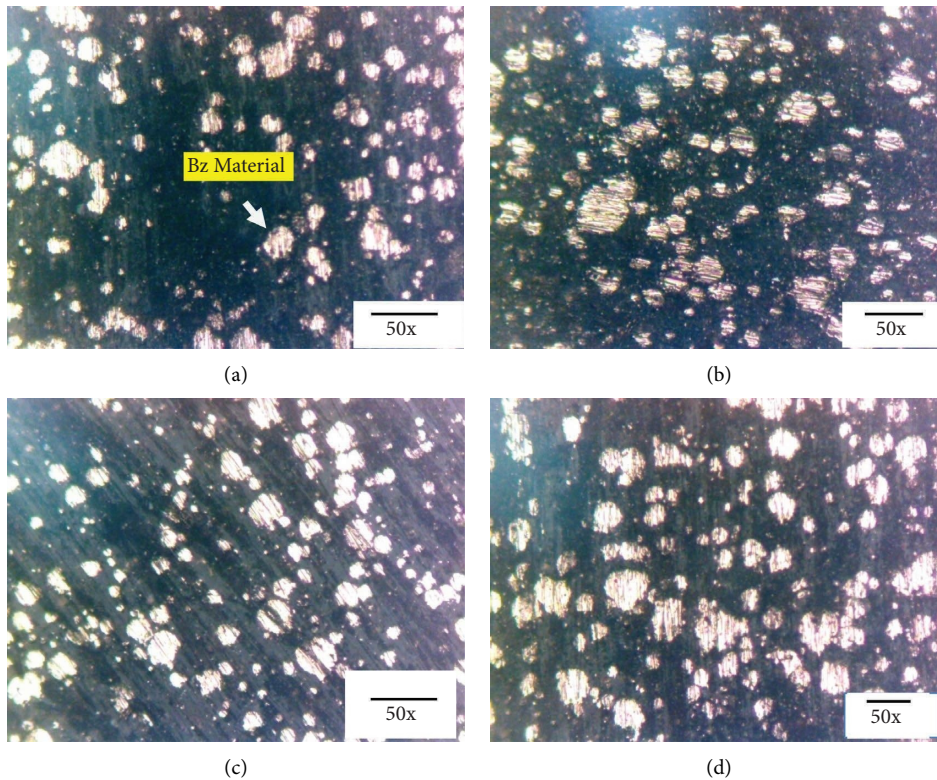


FIGURE 2: 3D composite filament and optical images of composite filament with varying % of Bz: (a) 6%; (b) 10%; (c) 14%; (d) 18%.

particles that may be more slippery and have lower ductility, reducing the tensile and bending strength of the test pieces. This activity directly affects the elongation properties of the combined sample. With the increase of Bz Wt% from 6% to 18%, nearly 300% filament property change is noted, demonstrating the influence of reinforcement in the matrix. Excessive surfaces of bronze particles resist the load before deformation, which increases the compressive strength of the specimen as reinforcement increases. From the analysis in Table 1, it may be concluded that bronze reinforcement with 14% would be an appropriate component of the matrix material. The influence of bronze change on composite filaments causes many printing problems.

3. Experimental Setup

The CNC LMW-JV55 vertical microcasting model is used for this study and is shown in Figure 3(a). Based on the previous study on PMC drilling, the independent parameters for the drilling machine are defined and shown in Table 2. In the present study, the experimental condition of the orthogonal matrix of Orthogonal Array of L27 Taguchi is calculated and performed.

The commercially available tungsten carbide drill bit of diameter 0.5, 0.7, and 0.9 mm, with the angle of the 45° flute is used in the present study. Among the considered blades (45°, 0°, and helical type), 45° blades exhibited the best drilling performance [28]. The dimensions of the printed sample are convenient to adapt to the working table of the CNC machine. An experiment is carried out to measure vibration during the machining process using acoustic sensors. The observations are dependent upon the rotation speed (200–2000 rev/min) vs. the feed (0.1 to 0.3 mm/min), which is recorded, which will not make a significant change to the machined samples. Samples are printed with and without holes; twisted bits are shown in Figure 3(b) with experimental configuration.

3.1. Delamination Percentage. Delamination is used to evaluate test samples under different machining conditions. The importance of delamination factors is measured using an optical test. Processing parameters are important for the surface quality of the drilled hole in terms of material removal rate (MRR) and time [29]. The delamination factor is the ratio between the maximum hole's diameter (D_{max}) and the nominal diameter (D_{nom}), as shown below

$$\text{Delamination factor } (F_D) = \frac{D_{max}}{D_{min}}, \quad (1)$$

$$\text{material removal rate (MRR)} = \frac{\pi}{4} * D^2 * f * N \frac{\text{mm}^3}{\text{min}}, \quad (2)$$

where D = diameter of the drill bit (mm); F = feed (mm/min); and N = spindle speed (rev/min).

4. Results and Discussion

4.1. Optical Microscopy Examination. To investigate the importance of the printed hole and the drilled hole on FDM quality measurement, the machined samples are subjected to an optical image. The image of the different drills is given in Table 3.

Optical microscopy examination is one of the simplest techniques to examine the machining effect on the test sample [30]. As the FDM parameters are dependent on the filament material, the decrease in the hole's geometry can cause severe damage to this surface due to layer build-up. As increasing the thickness of the layer can significantly reduce the flow of matter, defects cannot be neglected. Being the composite filament, as during the layer build-up, the density of Bz causes the change in layer thickness and provides a bulge shape projection over the inner surface of the printed whole. Achieving a right hole's thickness is almost impossible in FDM. Hence, a secondary processing operation such as microdrilling becomes necessary.

The decrease of the hole's diameter causes serious defects in the thickness of the hole's geometry, and it can be verified from Figure 3. While in microdrilling, surface defects such as burr formation, kerf taper, and shrinkage are noted. From the overall observation, it is very clear that an additional concentration should be made if the hole's dimension is less than 0.5 mm. To find out more about the drilled surface L27, Table 4 presents in different machining conditions, both at the point of entry and at the point of exit of the drilled hole. All the images are taken with 50x magnification. The removal rate and percentage of delamination are also considered in this study.

The overall observation in Table 5 can be summarised in the following way:

- (1) Observing the cut parameters indicates that the feed rate is critical to the PLA sample-14% Bz.
- (2) The delamination effect on the test sample layer by layer results in direct damage to the inner surface of the layer. This happens due to the working pressure existed by the tool bit on various layers printed on the FDM sample.
- (3) The force and mechanism cause the delamination area and provide the peel-off effect, which discriminates the entry portion of the drilled hole and affects the circumferences in the delamination zone as tools slide towards the exit portion.

The rotational speed, depth of cut, and cutting force may cause vibration during microdrilling. Besides, large thrust force given during the drilling operation at minimum spindle speed causes delamination. As the sample is built layer by layer, it has serious issue related to delamination. Also, the uneven material deposition and irregular particle dispersion during building the sample will increase the severity rate. Higher spindle speed with low feed rate will reduce the delamination failure for 3D printed samples. Based on the previous report, it could be established that the

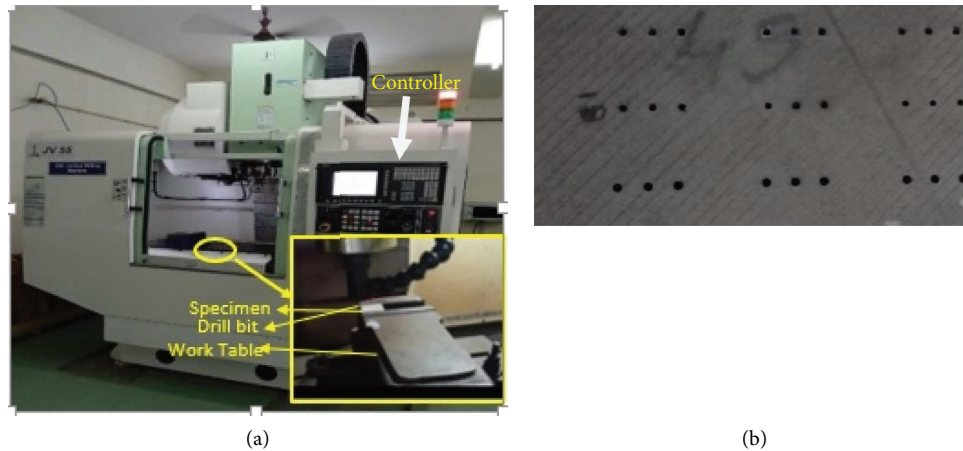


FIGURE 3: (a) Microdrilling set-up. (b) Drilling specimen.

TABLE 2: Experimental conditions.

Parameters	Levels		
	Level 1	Level 2	Level 3
Width of cut (mm)	0.5	0.7	0.9
Spindle speed (rpm)	2000	2500	3000
Feed (mm/min)	0.1	0.2	0.3

feed rate provides excessive faults relative to the spindle speed.

4.2. Surface Analysis. The surface topography of the samples constructed using drilled hole is analyzed by SEM. Figure 4 shows the SEM analysis of drilled and printed hole. The increase in cross-section is observed in the printing hole; however, the circularity is preserved for the drilled hole. Figures 4(a) and 4(b), taken from the upper and lower surface of the 0.9 mm drilled holes, confirm the circular nature of the holes. Through observation, it is clear that printing holes of more than 1 mm is recommended in 3D printing. A secondary machining operation is required to have a microcut hole. To know more about the cutting region, the drilled part was cut through the electric cutter, and the picture is shown in Figure 4(c). The inner surface of the machined sample at 0.7 mm and 0.5 mm is shown in Figures 4(d) and 4(e), respectively. Increasing the diameter of the tool increases the kerf angle along the inner side of the cutting zone. However, the chip that flows over the outer surface of the machine sample has enough force to remove the burrs that occur during the machining and makes a smooth machined surface, and it can be verified from Figure 4(d).

The presence of burrs and surface defects is clearly visible on the 0.5 mm hole cross-sectional surface. As the progression of the drill bit is small, there is a less chip withdrawal rate. Whatever the machining conditions, the reinforcements run off the surface of the materials and cause wear along the inner surface of the printed hole. To reduce the defects in drilling multiple pass with low

quantity lubrication is recommended [31]. The least generation of machining temperature can also lead to this fault for samples of drilled holes of 0.5 mm. The driving force and vibration occur during machining, which significantly affects the binding force between each layer and can be checked by Figure 4(f). Through visual inspection and based on the circularity obtained from Table 5 images, it can be stated that E27 machining condition will provide the defect-free component that is machined at the condition of drill diameter of 0.9 mm, speed of 3000 rpm, and feed rate of 0.1 mm, and it can be verified through Figure 4(g).

The bulk removal of PLA material is seen around the drilled holes, and at the same time, the reinforcement Bz particle has been pushed in the inner surface of the test sample. In addition, the height of the layer and the adequate dispersion of the Bz particles in the matrix are clearly recorded through Figure 4(h). Furthermore, the irregular state of machining can lead to holes of poor circularity and cause effects at the exit point of the nozzle. However, micromilling is essential even after performing drilling to improve the accuracy level. [32]. Furthermore, it causes mass removal of the material at the end of the cut. This can be seen from Figures 4(i) and 4(j).

4.3. Tool Wear Study. The effect of delamination is that it avoids the external force while drilling that exhibits the behaviour of the test sample and depends on the thickness of the sample and the size of the drill bit. The drill survey will provide the effect of the processing state, where the SEM images of the tools show the faults. Figure 5 shows the different magnification image of the 0.9 mm bit machined at 3000 rpm with a feed rate of 0.1 mm/min. Figure 5(a) shows the low magnification tool image where the PLA weld is on the surface of the tool. No severe defects are observed at the cutting edge of the tool. This is because of the smooth property of PLA matrix. However, the matrix property may increase the working temperature and cause severe distortion [33]. When the tool slides on the test sample, it increases the machining temperature which gradually reduces the

TABLE 3: Specification of a twist drill.

Set	Diameter (mm)	Description
1	0.5	Twist drills having three helical cutting lips with different diameters; point angle is 45°
2	0.7	
3	0.9	


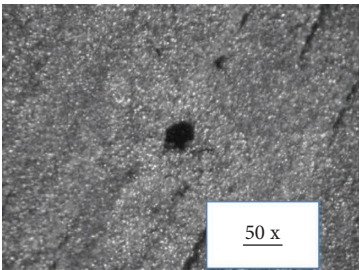
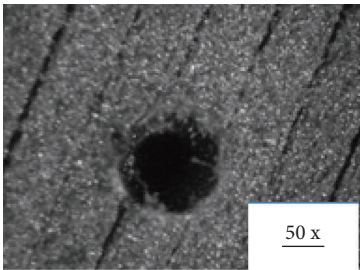
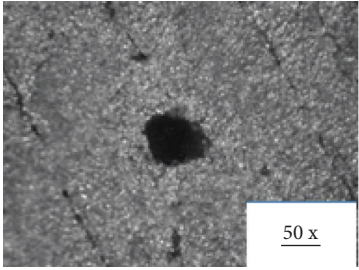
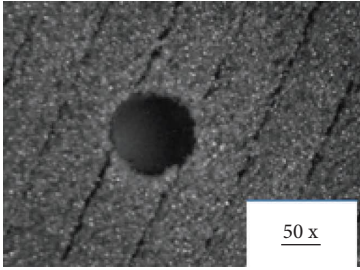
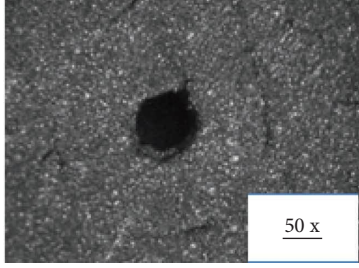
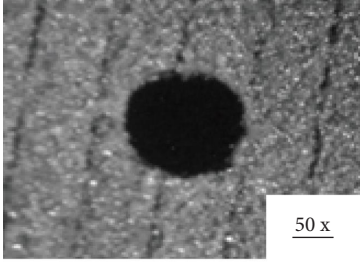


TABLE 4: The images of microholes printed and machined with three drill bits: (a) 0.5 mm; (b) 0.7 mm; (c) 0.9 mm.

Drill diameter (mm)	FDM printed samples	Drilled samples
0.5		
0.7		
0.9		

stiffness of the test material. This action causes the free movement of chips on the external surface of the tool. The reinforced Bz element that sticks to the PLA matrix glides smoothly on the tool without causing rupture or wear on the cutting surface on the tool side.

The nose of the tool has suffered serious damage mainly due to the reinforcing material. When in contact with hard frames, the high strength steel (HSS) tool is subjected to a heavy workload to remove the material. This may result in a tear on the nose area of the tool. The working effect on the geometry of the tool can be viewed through Figures 5(b) and 5(c). Under high working conditions, sudden wear and tear of the tool and loss of material around the nose are observed, and this is due to the clustered Bz particle. The wear zone of the tool and the reinforcing weld in the tool tip are illustrated in Figure 5(d).

The quality of the drill bit significantly affects the machining performance due to excessive force applied. The delamination effect of 0.5 mm is maximum at E8 condition at a material removal rate of $0.2757 \text{ mm}^3/\text{m}$ at a spindle speed of 3000 rpm and a feed rate of 0.2 mm/min. A 23% of

delamination factor are considered with maximum output; then, there is a chance of increasing the surface of the drilled hole. The vibration that occurs during the previous condition may cause a challenging affect to the researcher. The delamination effect of 0.7 mm drill bit was found to have maximum MRR of $0.5479 \text{ mm}^3/\text{min}$ at E12 conditions with a delamination effect of 12%. Here, the feed rate and the speed are 0.3 mm/min and 2000 rpm, respectively. At E27, the machining effect has shown the MRR of $1.1842 \text{ mm}^3/\text{min}$ with a 32% delamination factor. Here, the spindle speed and feed rate are recorded to be 3000 rpm and 0.3 mm/min, respectively, at E27 condition.

The study on the delamination effect during a micro-drilling operation on printed FDM samples concludes that the feed speed has a significant delamination effect, irrespective of drill diameter and spindle speed. Large diameter of the drill with a low spindle velocity will have an effect on the built layer. The minimum delamination was achieved when the low feed rate and the quality of the drill hole using the twist drill bit have been proven to be better than the brad drill bit [34]; a similar effect was noted in the present study.

TABLE 5: Microdrilling observations.

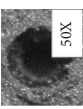
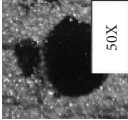
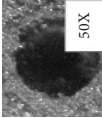
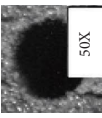
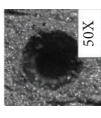
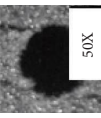
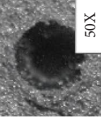
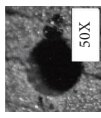
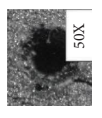
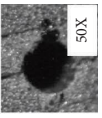
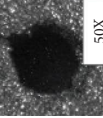
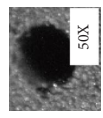
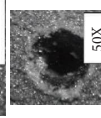
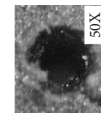
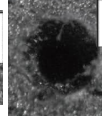
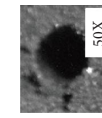
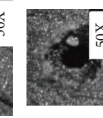
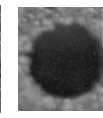
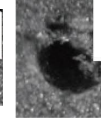
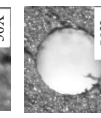
Ex. no	Entrance of a drill area	Exit of a drill area	MRR (mm^3/min)	Delamination percentage
E1			0.2092	13
E2			0.2409	12
E3			0.2983	18
E4			0.2166	13
E5			0.2843	24
E6			0.3246	24
E7			0.2208	17
E8			0.2757	23
E9			0.2660	9
E10			0.3673	8

TABLE 5: Continued.

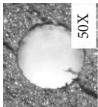
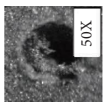
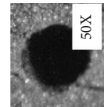
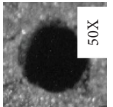
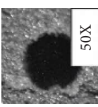
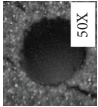
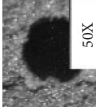
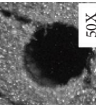
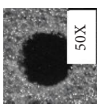
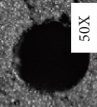
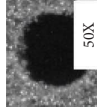
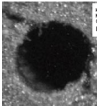
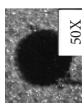
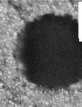
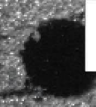
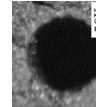
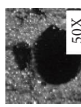
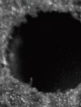
Ex. no	Entrance of a drill area	Exit of a drill area	MRR (mm ³ /min)	Delamination percentage
E11			0.4517	10
E12			0.5479	12
E13			0.3649	5
E14			0.4578	9
E15			0.5243	10
E16			0.3841	7
E17			0.4609	9
E18			0.5361	11
E19			0.7559	21
E20			0.9641	26

TABLE 5: Continued.

Ex. no	Entrance of a drill area	Exit of a drill area	MRR (mm ³ /min)	Delamination percentage
E21			1.0982	28
E22			0.8244	25
E23			0.9741	27
E24			1.1076	27
E25			0.8610	26
E26			1.0209	29
E27			1.1842	32

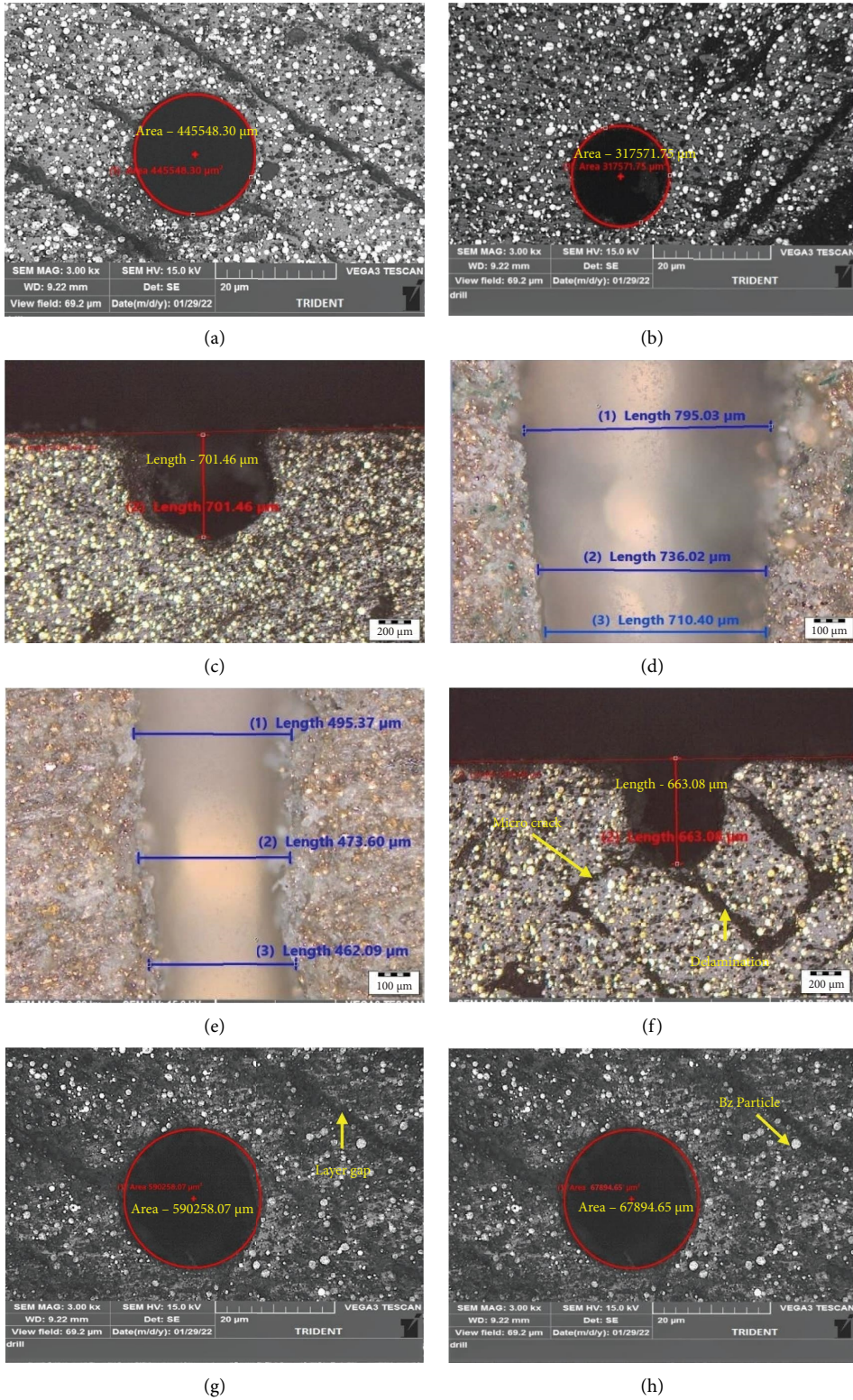


FIGURE 4: Continued.

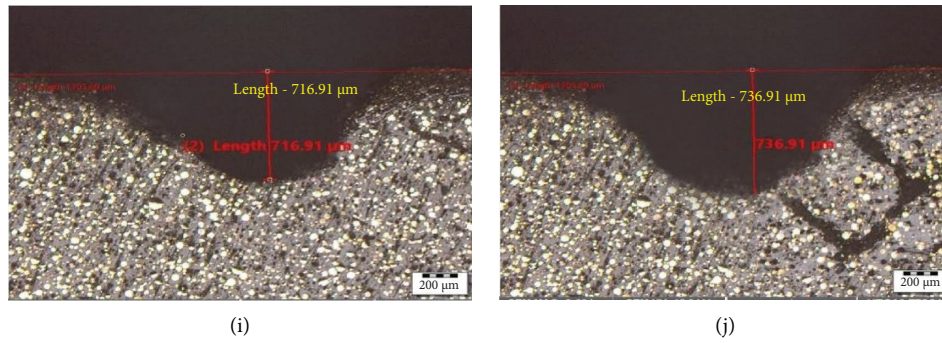


FIGURE 4: SEM image of the drilled hole at various machine conditions.

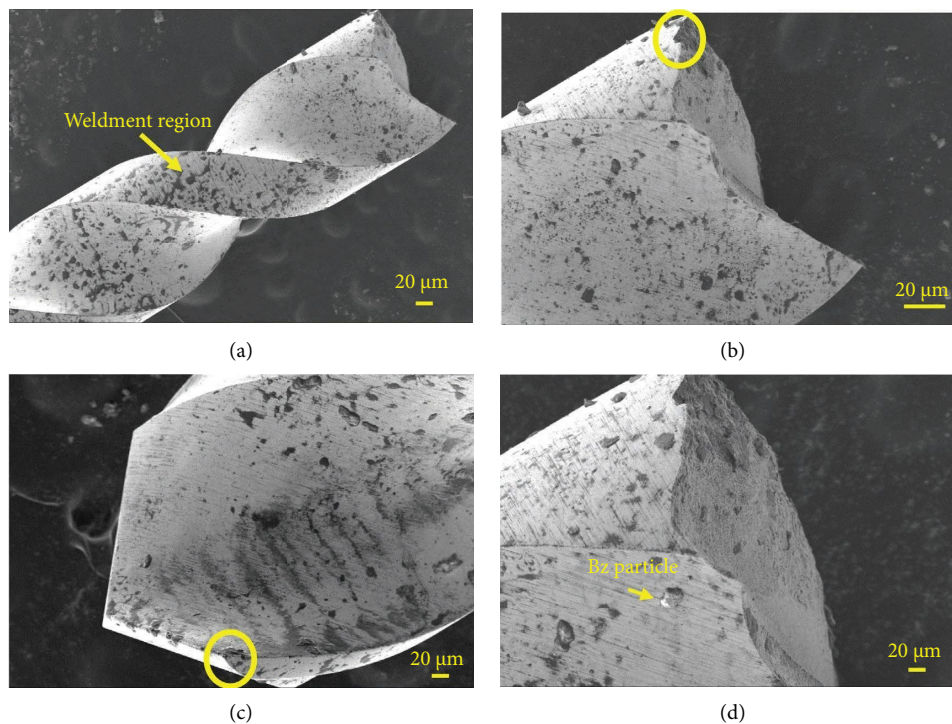


FIGURE 5: Tool condition at different positions in drilling operation.

5. Conclusion

This study explains the microdrilling behaviour of PLA-Bz composites which specifies the quality of the microholes. Observations concerning the percentage of delamination with various drilling parameters and the roundness of the hole in and out surface are reported. The delaminating effect is evaluated to characterize the damage in the microdrilled holes. Based on the results, the delamination factors are obtained with feed speed and feed rate. The results are explained with defects which have occurred due to feed speed and composite width. The structural zone improves the correct tolerance by means of speed and feed speed. This reduces the delaminating zone and improves the improvement of the drilled hole. The printing conditions of the identified samples are obtained

for the processing of a microdrilling, and the conclusion is given as follows:

- (1) The circularity of the drilled hole is retained at high speed conditions because increase in working temperature causes free-flow of chips along the tool surface
- (2) Delamination effects are greatly affected by the size of holes of 0.5, 0.7, and 0.9 mm
- (3) The velocity factor is greatly influenced by machining conditions, with a higher feed rate and a lower material removal rate
- (4) At 0.9 mm diameter, the maximum delamination effect at condition E27 is achieved by comparing the different microdrilled diameters

- (5) Feed, speed, and cutting width are highly influenced by MRR with efficient drilled holes.

Data Availability

No data were used to support the findings of this study.

Conflicts of Interest

The authors declare that they have no conflicts of interest.

Acknowledgments

The authors are grateful to the Centre of Excellence, VFSTR (Deemed to be University) for the support to finish this innovative study.

References

- [1] D. Meinhard, A. Haeger, and V. Knoblauch, "Drilling induced defects on carbon fiber-reinforced thermoplastic polyamide and their effect on mechanical properties," *Composite Structures*, vol. 256, Article ID 113138, 2021.
- [2] B. Ameri, F. Taheri-Behrooz, and M. R. M. Aliha, "Evaluation of the geometrical discontinuity effect on mixed-mode I/II fracture load of FDM 3D-printed parts," *Theoretical and Applied Fracture Mechanics*, vol. 113, Article ID 102953, 2021.
- [3] B. Zhang, T. Sui, B. Lin et al., "Drilling process of Cf/SiC ceramic matrix composites: cutting force modeling, machining quality and PCD tool wear analysis," *Journal of Materials Processing Technology*, vol. 304, Article ID 117566, 2022.
- [4] F. Paliling, A. Y. Aminy, and H. Arsyad, "The effect of machine process in two flute end mill feeding rate on delamination in carbon fiber reinforced polymer materials," in *Proceedings of the AIP Conference Proceedings*, vol. 2384, pp. 1–040003, AIP Publishing LLC, Surabaya, Indonesia, December 2021.
- [5] F. Henson, H. Lydon, M. Birch, R. Brooks, and A. McCaskie, "Using apheresis-derived cells to augment micro-drilling in the treatment of chondral defects in an ovine model," *Journal of Orthopaedic Research*, vol. 39, no. 7, pp. 1411–1422, 2021.
- [6] S. A. Niknam, B. Davoodi, and V. Songmene, "Milling Al520-MMC reinforced with SiC particles and Additive elements Bi and Sn," *Materials*, vol. 15, p. 4, 2022.
- [7] S. A. Arhamnamazi, F. Aymerich, P. Buonadonna, and M. E. Mehtedi, "Assessment of drilling-induced delamination and tool wear in carbon fibre reinforced laminates," *Polymers and Polymer Composites*, vol. 29, pp. S729–S740, 2021.
- [8] M. R. Choudhury and K. Debnath, "Machining of bio-composites," in *Advances in Machining of Composite Materials*, pp. 421–457, Springer, Cham, Switzerland, 2021.
- [9] J. C. Su, G. Bettin, S. Buerger et al., "Direct subsurface measurements through precise micro drilling," Technical Report (No. SAND2021-11690), Sandia National Lab.(SNL-NM), Albuquerque, NM, USA, 2021.
- [10] S. Rawal, A. M. Sidpara, and J. Paul, "A review on micro machining of polymer composites," *Journal of Manufacturing Processes*, vol. 77, pp. 87–113, 2022.
- [11] M. S. S. Saravanan, V. Ananda, S. P. K. Babu et al., "Properties evaluation of electroless Ni-coated low-carbon steels," *Journal of Nanomaterials*, vol. 2022, Article ID 8497927, 8 pages, 2022.
- [12] N. Ramanujam, S. Dhanabalan, D. Raj Kumar, and N. Jeya Prakash, "Investigation of micro-hole quality in drilled CFRP laminates through CO2 laser," *Arabian Journal for Science and Engineering*, vol. 46, no. 8, pp. 7557–7575, 2021.
- [13] D. R. Tripathi, K. H. Vachhani, D. Bandhu, S. Kumari, V. R. Kumar, and K. Abhishek, "Experimental investigation and optimization of abrasive waterjet machining parameters for GFRP composites using metaphor-less algorithms," *Materials and Manufacturing Processes*, vol. 36, no. 7, pp. 803–813, 2021.
- [14] J. H. Lee, J. C. Ge, and J. H. Song, "Study on burr formation and tool wear in drilling CFRP and its hybrid composites," *Applied Sciences*, vol. 11, no. 1, p. 384, 2021.
- [15] A. Yazdanfar and H. Shahrajabian, "Experimental investigation of multi-wall carbon nanotube added epoxy resin on the EDM performance of epoxy/carbon fiber/MWCNT hybrid composites," *The International Journal of Advanced Manufacturing Technology*, vol. 116, no. 5-6, pp. 1801–1817, 2021.
- [16] S. Balaji, P. Maniarasan, S. V. Alagarsamy et al., "Optimization and prediction of tribological behaviour of Al-FeSi alloy-based nanograin-refined composites using Taguchi with response surface methodology," *Journal of Nanomaterials*, vol. 2022, Article ID 9733264, 12 pages, 2022.
- [17] V. M. Pavan, K. Balamurugan, and L. Tp, "PLA-Cu reinforced composite filament: preparation and flexural property printed at different machining conditions," *Advanced Composite Materials*, vol. 31, no. 1, pp. 102–117, 2022.
- [18] M. V. Pavan, K. Balamurugan, V. Srinivasadesikan, and S. L. Lee, "Impact and shear behavior of PLA/12% Cu reinforced composite filament printed at different FDM conditions," *Arabian Journal for Science and Engineering*, vol. 46, no. 12, pp. 12709–12720, 2021.
- [19] A. Ünüvar, M. Koyunbakan, and M. Bagci, "Optimization and effects of machining parameters on delamination in drilling of pure and Al2O3/SiO2-added GFRP composites," *The International Journal of Advanced Manufacturing Technology*, vol. 119, no. 1-2, pp. 657–675, 2022.
- [20] M. M. Sarafraz and F. C. Christo, "Thermal and flow characteristics of liquid flow in a 3D-printed micro-reactor: a numerical and experimental study," *Applied Thermal Engineering*, vol. 199, Article ID 117531, 2021.
- [21] K. M. John, S. Thirumalai Kumaran, R. Kurniawan, and F. Ahmed, "Evaluation of thrust force and delamination in drilling of CFRP by using active spring restoring backup force," *Materials Today: Proceedings*, vol. 49, pp. 269–274, 2022.
- [22] A. T. Erturk, F. Vatanserver, E. Yazar, E. A. Guven, and T. Sinmazcelik, "Effects of cutting temperature and process optimization in drilling of GFRP composites," *Journal of Composite Materials*, vol. 55, no. 2, pp. 235–249, 2021.
- [23] U. A. Khashaba, M. S. Abd-Elwahed, M. A. Eltahir, I. Najjar, A. Melaibari, and K. I. Ahmed, "Thermo-mechanical and delamination properties in drilling GFRP composites by various drill angles," *Polymers*, vol. 13, p. 1884, 2021.
- [24] F. W. Panella and A. Pirinu, "Fatigue and damage analysis on aeronautical CFRP elements under tension and bending loads: two cases of study," *International Journal of Fatigue*, vol. 152, Article ID 106403, 2021.
- [25] M. Mukhtar, M. Effendee, M. H. Ibrahim, and M. Syahrir, "Analysis of solid carbide drilling performance on AISI 316L austenite stainless steel using MQL (minimum quantity lubrication) using peck drilling approach," in *Proceedings of the*

- Journal of Physics: Conference Series*, vol. 1874, no. 1, December 2021.
- [26] T. V. Rajamurugan, C. Rajaganapathy, S. P. Jani, C. S. Gurram, H. L. Allasi, and S. Z. Damtew, "Analysis of drilling of coir fiber-reinforced polyester composites using multifaceted drill bit," *Advances in Materials Science and Engineering*, vol. 2022, Article ID 9481566, 9 pages, 2022.
- [27] K. Balamurugan, G. Kalusuraman, and P. Sneha, "Evaluation of flexural and shear property of high performance PLA/Bz composite filament printed at different FDM parametric conditions," *International Journal of High Performance Systems Architecture*, vol. 10, no. 3/4, pp. 119–127, 2021.
- [28] S. Park, B. Ko, H. Lee, and H. So, "Rapid manufacturing of micro-drilling devices using FFF-type 3D printing technology," *Scientific Reports*, vol. 11, no. 1, pp. 12179–9, 2021.
- [29] V. G. Ladeesh and R. Manu, "Grinding aided electrochemical discharge drilling (G-ECDD): a theoretical analysis and mathematical modelling of material removal rate," *Journal of the Brazilian Society of Mechanical Sciences and Engineering*, vol. 43, no. 9, pp. 422–520, 2021.
- [30] S. Nazari-Onlaghi, A. Sadeghi, and M. Karimpour, "Design and manufacture of a micro-tensile testing machine for in situ optical observation and DIC analysis: application to 3D-printed and compression-molded ABS," *Journal of Micro-mechanics and Microengineering*, vol. 31, no. 4, Article ID 045016, 2021.
- [31] N. M. Cococetta, D. Pearl, M. P. Jahan, and J. Ma, "Investigating surface finish, burr formation, and tool wear during machining of 3D printed carbon fiber reinforced polymer composite," *Journal of Manufacturing Processes*, vol. 56, pp. 1304–1316, 2020.
- [32] A. Das, D. Barrenkala, K. Debnath, P. Kumar, R. Rajan, and S. K. Patel, "Comparative assessments of machining forces in 3D printed polymer composite during milling operation using two coated carbide end mills," *Materials Today: Proceedings*, vol. 62, pp. 6107–6114, 2022.
- [33] C. Y. Wang, Y. H. Chen, Q. L. An, X. J. Cai, W. W. Ming, and M. Chen, "Drilling temperature and hole quality in drilling of CFRP/aluminum stacks using diamond coated drill," *International Journal of Precision Engineering and Manufacturing*, vol. 16, no. 8, pp. 1689–1697, 2015.
- [34] A. Ngah, S. D. Salman, Z. Leman, S. Sapuan, M. Alkbir, and F. Januddi, "Effects of drilling parameters on delamination of kenaf-glass fibre reinforced unsaturated polyester composites," *Journal of Industrial Textiles*, vol. 51, pp. 3057S–3076S, 2022.